The 8th European Congress on Computational Methods in Applied Sciences and Engineering
ECCOMAS Congress 2022
5–9 June 2022, Oslo, Norway

VALIDATION ON A NEW ANISOTROPIC FOUR-PARAMETER TURBULENCE MODEL FOR LOW PRANDTL NUMBER FLUIDS

G. Barbi[1], A. Chierici[2], V. Giovacchini[1], S. Manservisi[1] and L. Sirotti[1*]

[1] University of Bologna - DIN, Via dei Colli 16, 40136 Bologna (BO), Italy
[2] Department of Mathematics and Statistics, Texas Tech University, TX, USA
*e-mail: lucia.sirotti4@unibo.it

Key words: low-Prandtl number fluids, liquid metals, turbulent heat transfer, anisotropy, Reynolds-stress tensor

Abstract. *This work aims to validate a new anisotropic four-parameter turbulence model for low-Prandtl number fluids in forced and mixed convection. Traditional models based on the gradient-diffusion hypothesis and Reynolds analogy are inadequate to simulate the turbulent heat transfer in low-Prandtl number fluids. Additional transport equations for thermal variables are required to predict the characteristic thermal time scale. In a four-parameter turbulence model, two additional transport equations are solved for the temperature variance and its dissipation rate. Thus, it is possible to formulate appropriate characteristic time scales to predict the near-wall and bulk behaviour of mean and turbulent variables. The isotropic version of the four-parameter model has been widely studied and validated in forced and mixed convection. We aim to extend the model validity by proposing explicit algebraic models for the closure of Reynolds stress tensor and turbulent heat flux. For the validation of the anisotropic four-parameter turbulence model, low-Prandtl number fluids are simulated in several flow configurations considering buoyancy effects and numerical results are compared with DNS data.*

1 INTRODUCTION

Among the most promising technological innovations in the energy field, the usage of liquid metals as heat transport fluids is central. In this respect, the large temperature ranges over which they remain liquid, and their high thermal conductivity, make them attractive as a viable alternative to conventional heat transport fluids [1]. Due to their thermal properties, these materials are particularly suitable for applications involving high thermal loads, such as concentrated solar power plants [2, 3] and Generation IV nuclear reactors [4, 5]. The design of complex systems can not be separated from a numerical and computational approach, and Computational Fluid Dynamics tools are required for an accurate prediction of the thermal-hydraulics behavior. Nevertheless, the modelling of turbulent heat flux in liquid metals, as low-Prandtl number fluids, can not be easily achieved using the commercial CFD codes. Therefore, in the framework of the Reynolds-Averaged Navier-Stokes (RANS) approach, the study of accurate and robust computational techniques to deal with this problem is currently in the development phase, and the closure of the RANS system is still challenging.

Over the years, different models have been proposed to achieve the closure of the momentum equation. First-order models are based on the Boussinesq assumption that involves a linear dependence between the Reynolds stress tensor and the mean rate of deformation tensor S_{ij} through an isotropic eddy viscosity ν_t. On the other hand, the second-order models define the transport equation for each component of the Reynolds stress tensor. The former show some deficiencies when anisotropic behavior occurs, while the latter, despite being more accurate, require a higher numerical effort. In this work, for the closure of the momentum equation, we propose an Explicit Algebraic Stress Model (EASM) which belongs to a class of models between first and second-order. As concerns the turbulent heat flux modelling, only a few models have been developed and validated. The almost universally employed models are based on the Simple Gradient Diffusion Hypothesis (SGDH) and rely on the similarity between the turbulent heat flux and the molecular heat conduction. Furthermore, the Reynolds Analogy is often invoked to evaluate the unknown turbulent thermal diffusivity α_t, which is considered to be proportional to the eddy viscosity, with the inverse of a constant turbulent Prandtl number as a proportionality factor. This approach delivers reasonable results in the forced convection regime and for fluids with $Pr \simeq 1$, however, it does not hold for applications involving non-unity Prandtl number fluids especially in mixed convection regimes when buoyancy effects have to be accounted for [6]. In order to overcome these limits, we have adopted an Explicit Algebraic Heat Flux Model (EAHFM) for the closure of the energy equation, which is derived starting from the class of implicit Algebraic Heat Flux Models [7, 8]. In this work, the above-mentioned anisotropic models are coupled with the logarithmic four-parameter turbulence model proposed in [9, 10, 11, 12], which solves the transport equation for each of the turbulent variables K-Ω-K_θ-Ω_θ.

In order to validate the proposed anisotropic four-equation turbulence model, we have considered the turbulent flow of liquid sodium over a vertical backward-facing step. This flow is extensively used in many devices, such as the in-and-outflow of thermal storage containers in power conversion systems. Because of its importance, it has been widely investigated in the literature and several DNS simulations for different flow regimes are available for the comparison and validation of turbulence models [13, 14, 15, 16]. The anisotropic four-equation model is presented in Section 2, while in Section 3 the solution of the above-mentioned anisotropic

turbulent model is compared with the results obtained for the isotropic four-equation model. These results are discussed in comparison with literature data.

2 MATHEMATICAL MODEL

The governing equations to be solved for an incompressible Newtonian fluid in a turbulent flow regime are the Reynolds-averaged conservation equations of mass, momentum, and energy. In order to simulate the mixed convection regime, the Navier Stokes equations are coupled together with the energy equation through the Oberbeck-Boussinesq approximation. This set of equations is known as RANS system, namely

$$\frac{\partial u_i}{\partial x_i} = 0\,, \tag{1}$$

$$\frac{\partial u_i}{\partial t} + u_j \frac{\partial u_i}{\partial x_j} = -\frac{1}{\rho}\frac{\partial p}{\partial x_i} + \frac{\partial}{\partial x_j}\left[\nu\left(\frac{\partial u_i}{\partial x_j} + \frac{\partial u_j}{\partial x_i}\right) - \langle u_i' u_j' \rangle\right] - g_i \beta (T - T_0)\,, \tag{2}$$

$$\frac{\partial T}{\partial t} + u_j \frac{\partial T}{\partial x_j} = \frac{\partial}{\partial x_j}\left(\alpha \frac{\partial T}{\partial x_j} - \langle u_j' T' \rangle\right), \tag{3}$$

where u_i, p and T are the mean quantities, while u_i' and T' are the fluctuating fields. The constant ν is the kinematic viscosity, α is the thermal diffusivity, ρ is the fluid density, and β is the thermal expansion coefficient. Compared to the instantaneous fields equations, the averaging operation introduces additional unknowns, meaning the six components of the symmetric Reynolds stress tensor $\langle u_i' u_j' \rangle$ and the three components of the turbulent heat flux $\langle u_i' T' \rangle$. The resulting system is no longer a closed problem, and models must be introduced in order to determine these unknown quantities.

Since the first-order models are inadequate to capture the anisotropy of the flows and the second-order models increase the numerical effort, the Reynolds stress tensor is modelled using an Explicit Algebraic Stress Model (EASM). This nonlinear eddy viscosity model is obtained by applying the local equilibrium hypothesis between production and dissipation to the full transport equation for $\langle u_i' u_j' \rangle$. Defined the strain-rate tensor as $S_{ij} = \frac{1}{2}(\frac{\partial u_i}{\partial x_j} + \frac{\partial u_j}{\partial x_i})$ and the vorticity tensor as $\Omega_{ij} = \frac{1}{2}(\frac{\partial u_i}{\partial x_j} - \frac{\partial u_j}{\partial x_i})$, the Reynolds stress tensor can be computed as follows [17]

$$\langle u_i' u_j' \rangle = \frac{2}{3} k \delta_{ij} - \frac{2\nu_t}{f_R} S_{ij} - \frac{4 C_D k f_\tau}{f_R}\left(S_{ik}\Omega_{kj} - \Omega_{ik} S_{kj} - S_{ik} S_{kj} + \frac{1}{3} S^2 \delta_{ij}\right). \tag{4}$$

The eddy viscosity ν_t can be expressed as a function of the turbulent kinetic energy k and a characteristic dynamical time scale τ_{lu}. Hence, the eddy viscosity is defined as $\nu_t = C_\mu f_\mu k \tau_{lu}$. The model constant C_μ takes the standard value 0.09 and the damping function f_μ is modelled using the formulation given by [17] as $f_\mu = 1 - \exp[-(R_d/26)^2]$, where $R_d = \upsilon y_d/\nu$ is the non-dimensional wall-distance, with $\upsilon = (\nu\varepsilon)^{\frac{1}{4}}$ that represents the Kolmogorov velocity scale and y_d the wall distance at a point, namely, the distance between that point and nearest point on the wall surfaces. The dynamical time scale is usually defined using the scale of energy-containing eddies $\tau_u = k/\varepsilon$, where ε is the dissipation rate. However, to consider the dissipation eddies

effect near the wall the time scale is corrected as follows

$$\tau_{lu} = \tau_u \left\{ 1 + \frac{35}{R_t^{\frac{3}{4}}} \exp\left[-\left(\frac{R_t}{30} \right)^{\frac{3}{4}} \right] \right\}, \tag{5}$$

where $R_t = k^2/(\nu\varepsilon)$ is the turbulent Reynolds number. The constant C_D is set to 0.8 and the function f_R is expressed as $f_R = 1 + 22/3(C_D\tau_{R_0})^2\Omega^2 + 2/3(C_D\tau_{R_0})^2(\Omega^2 - S^2)f_B$, where $S^2 = S_{mn}S_{mn}$, $\Omega^2 = \Omega_{mn}\Omega_{mn}$ and $f_B = 1 + C_\eta(C_D\tau_{R_0})^2(\Omega^2 - S^2)$. The function f_τ is introduced to take into account the wall-limiting behavior and anisotropy of the Reynolds normal stress components near the wall, and it is given by $f_\tau = \tau_{R_0}^2 + \tau_{R_W}^2$. The above-mentioned function depends on the characteristic time scale $\tau_{R_0} = \nu_t/k$ and the wall reflection time scale τ_{R_W}, defined by the expression [18]

$$\tau_{R_W} = \sqrt{\frac{f_R}{6C_D f_{S\Omega}}} \left(1 - \frac{3C_{v1}f_{v2}}{8} \right) f_{v1}^2 \,, \tag{6}$$

where

$$f_{v1} = \exp(-R_{tm}^2/2025), \tag{7}$$

$$f_{v2} = 1 - \exp(-\sqrt{R_t/C_{v2}}), \tag{8}$$

$$f_{S\Omega} = \frac{\Omega^2}{2} + \frac{S^2}{3} - \left| \sqrt{\frac{S^2}{2}} - \sqrt{\frac{\Omega^2}{2}} \right| \exp(-R_{tm}^2), \tag{9}$$

and the modified Reynolds number $R_{tm} = C_{tm}R_d R_t^{0.25}/(C_{tm}R_t^{0.25} + R_d)$. The other model constants are $C_\eta = 5$, $C_{v1} = 0.4$, $C_{v2} = 2000$ and $C_{tm} = 130$.

In this work, the turbulent heat flux is modelled using the Explicit Algebraic Heat Flux Model (EAHFM), which allows overcoming the limits of the first-order models and the Reynolds analogy. Indeed, in the proposed model, the turbulent heat flux $\langle u_i' T' \rangle$ is not necessarily parallel to the mean temperature gradient, which is, by contrast, peculiar to the SDGH model. Starting from the transport equation for the turbulent heat flux and imposing the hypothesis of the local equilibrium state between the production and the dissipation contributions [19] the following explicit algebraic expression can be derived [18]

$$\langle u_i' T' \rangle = -\frac{C_{t1}}{f_{RT}}\tau_m \Big[\langle u_i' u_j' \rangle \frac{\partial T}{\partial x_j} - \tau_m [(C_{t2} - C_{t3})S_{ij} + (C_{t2} - C_{t3})\Omega_{ij}] \langle u_j' u_k' \rangle \frac{\partial T}{\partial x_k} \Big] - \frac{2C_{t4}\tau_m}{f_{RT}} \delta_{ik} g_k \beta k_\theta \,. \tag{10}$$

Since the above-mentioned local equilibrium hypothesis does not work in the near-wall region, the characteristic thermal time scale τ_m modelling becomes relevant for correctly predicting the heat transfer in wall flows. Therefore, the thermal time scale τ_m is modelled using the expression introduced by [9, 10]

$$\tau_m = \tau_u f_{1t} \left(\frac{1}{Pr_t} + \frac{2R}{R + C_\gamma} f_{2t} + 1.3 \frac{\sqrt{2R}}{Pr R_t^{\frac{3}{4}}} f_{3t} \right), \tag{11}$$

where $R = (\varepsilon/k)/(\varepsilon_\theta/k_\theta)$ is the thermal to mechanical turbulent time scale ratio. The model constants and the model functions are reported in Table 1.

C_γ	C_{t1}	C_{t2}	C_{t3}	Pr_t
$0.25/Pr^{\frac{1}{4}}$	0.18	0.18	0.02	1.3
	f_{1t}		f_{2t}	f_{3t}
$[1-\exp(-\frac{R_d}{14})][1-\exp(-\frac{\sqrt{Pr}R_d}{14})]$			$\exp[-(\frac{R_t}{500})^2]$	$\exp[-(\frac{R_t}{200})^2]$
f_{RT}				
$1+0.5\tau_m^2[(C_{t2}+C_{t3})^2\Omega^2-(C_{t2}-C_{t3})^2S^2]$				

Table 1: Model constants and functions for Explicit Algebraic Heat Flux Model (10)-(11).

For the closure of the EASM model, the turbulent kinetic energy k and its specific dissipation rate ω, where $\omega = \varepsilon/(C_\mu k)$, are evaluated using the logarithmic turbulence model K-Ω [10, 12]. This logarithmic model helps to enhance the numerical stability if compared to the standard k-ω model because the state variables are always maintained positive during the solution process. The transport equations for the logarithmic variables $K = \ln(k)$ and $\Omega = \ln(\omega)$, used for the closure of the dynamical fields, are reported below

$$\frac{DK}{Dt} = \frac{\partial}{\partial x_i}\left[\left(\nu + \frac{\nu_t}{\sigma_k}\right)\frac{\partial K}{\partial x_i}\right] + \left(\nu + \frac{\nu_t}{\sigma_k}\right)\frac{\partial K}{\partial x_i}\frac{\partial K}{\partial x_i} + \frac{P_k}{e^K} + C_b\frac{P_b}{e^K} - C_\mu e^\Omega\,, \tag{12}$$

$$\begin{aligned}\frac{D\Omega}{Dt} = \frac{\partial}{\partial x_i}\left[\left(\nu + \frac{\nu_t}{\sigma_\omega}\right)\frac{\partial \Omega}{\partial x_i}\right] + \left(\nu + \frac{\nu_t}{\sigma_\omega}\right)\frac{\partial \Omega}{\partial x_i}\frac{\partial \Omega}{\partial x_i} + 2\left(\nu + \frac{\nu_t}{\sigma_\omega}\right)\frac{\partial K}{\partial x_i}\frac{\partial \Omega}{\partial x_i} + \\ + \frac{P_k}{e^K}(C_{\varepsilon 1}-1) + (C_b-1)\frac{P_b}{e^K} - C_\mu(C_{\varepsilon 2}f_\varepsilon - 1)e^\Omega\,,\end{aligned} \tag{13}$$

where $P_k = -\langle u_i' u_j'\rangle \partial u_i/\partial x_j$ is the production rate of turbulent kinetic energy and $P_b = -\beta g_i \langle u_i' T'\rangle$ is the source term for buoyant flows.

On the other hand, we have handled the closure of the turbulent heat flux, adding to the system of equations two additional transport equations for the evaluation of the mean temperature fluctuations k_θ and the specific dissipation rate ω_θ, where $\omega_\theta = \varepsilon_\theta/(C_\mu k_\theta)$ [10, 12]. As before, we propose a logarithmic turbulence model given by

$$\frac{DK_\theta}{Dt} = \frac{\partial}{\partial x_i}\left[\left(\alpha + \frac{\alpha_t}{\sigma_{k\theta}}\right)\frac{\partial K_\theta}{\partial x_i}\right] + \left(\alpha + \frac{\alpha_t}{\sigma_{k\theta}}\right)\frac{\partial K_\theta}{\partial x_i}\frac{\partial K_\theta}{\partial x_i} + \frac{P_{k_\theta}}{e^{K_\theta}} - C_\mu e^{\Omega_\theta}\,, \tag{14}$$

$$\begin{aligned}\frac{D\Omega_\theta}{Dt} = \frac{\partial}{\partial x_i}\left[\left(\alpha + \frac{\alpha_t}{\sigma_{\omega_\theta}}\right)\frac{\partial \Omega_\theta}{\partial x_i}\right] + \left(\alpha + \frac{\alpha_t}{\sigma_{\omega_\theta}}\right)\frac{\partial \Omega_\theta}{\partial x_i}\frac{\partial \Omega_\theta}{\partial x_i} + 2\left(\alpha + \frac{\alpha_t}{\sigma_{\omega_\theta}}\right)\frac{\partial K_\theta}{\partial x_i}\frac{\partial \Omega_\theta}{\partial x_i} + \\ + \frac{P_{k_\theta}}{e^{K_\theta}}(C_{p1}-1) + C_{p2}\frac{P_k}{e^K} - (C_{d1}-1)C_\mu e^{\Omega_\theta} - C_{d2}C_\mu e^\Omega\,,\end{aligned} \tag{15}$$

where $P_{k_\theta} = -\langle u_j' T'\rangle \partial T/\partial x_j$ and $\alpha_t = C_\theta k \tau_m$ is the eddy thermal diffusivity, with $C_\theta = 0.1$. The other model constants and model functions are reported in Table 2.

$C_{\varepsilon 1}$	$C_{\varepsilon 2}$	C_b	$\sigma_k = \sigma_\omega$	f_ε
1.9	1.5	1.44	1.4	$\{1 - 0.3\exp[-(R_t/6.5)^2]\}\{1 - \exp[-(R_d/3.7)^2]\}$
C_{p1}	C_{p2}	C_{d1}	$\sigma_{k\theta} = \sigma_{\omega\theta}$	C_{d2}
1.025	0.9	1.1	1.4	$\{1.9[1 - 0.3\exp[-(R_t/6.5)^2]] - 1\}\{1 - \exp[-(R_d/5)^2]\}$

Table 2: Constants and functions for the logarithmic four-parameter model (12)-(13)-(14)-(15).

3 NUMERICAL RESULTS

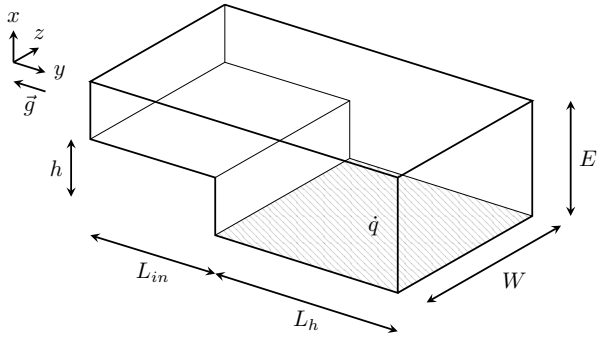

Figure 1: Representative sketch of backward-facing step geometry.

L_{in}/h	L_h/h	W	E_r	Re	Ri	Pr
2	20	0	1.5	9610	$0 - 0.338$	0.0088

Table 3: Geometrical parameters of the simulated domain.

In this section, we investigate the simulation results of a turbulent flow of liquid sodium over a vertical backward-facing step, solved with the in-house finite element code FEMuS [20]. In particular, the obtained results are reported for two different flow configurations: first, for forced convection regime with Richardson number $Ri = g\beta\Delta Th/U_b^2$ equal to zero, and second, for mixed convection regime with $Ri = 0.338$. In Figure 1 the reference domain [14] is reported as a representative sketch and its geometrical parameters are reported in Table 3. Here L_{in} is the inlet section length, h is the step height, W is the domain width and $E_r = E/(E-h)$ is the expansion ratio, where E is the downstream channel height.

As regards the boundary conditions, for the velocity field a fully developed inflow condition is imposed at the inlet section, and an outflow boundary condition is set at the outlet section. All the other boundaries are treated as no slip walls. Concerning the temperature, a uniform

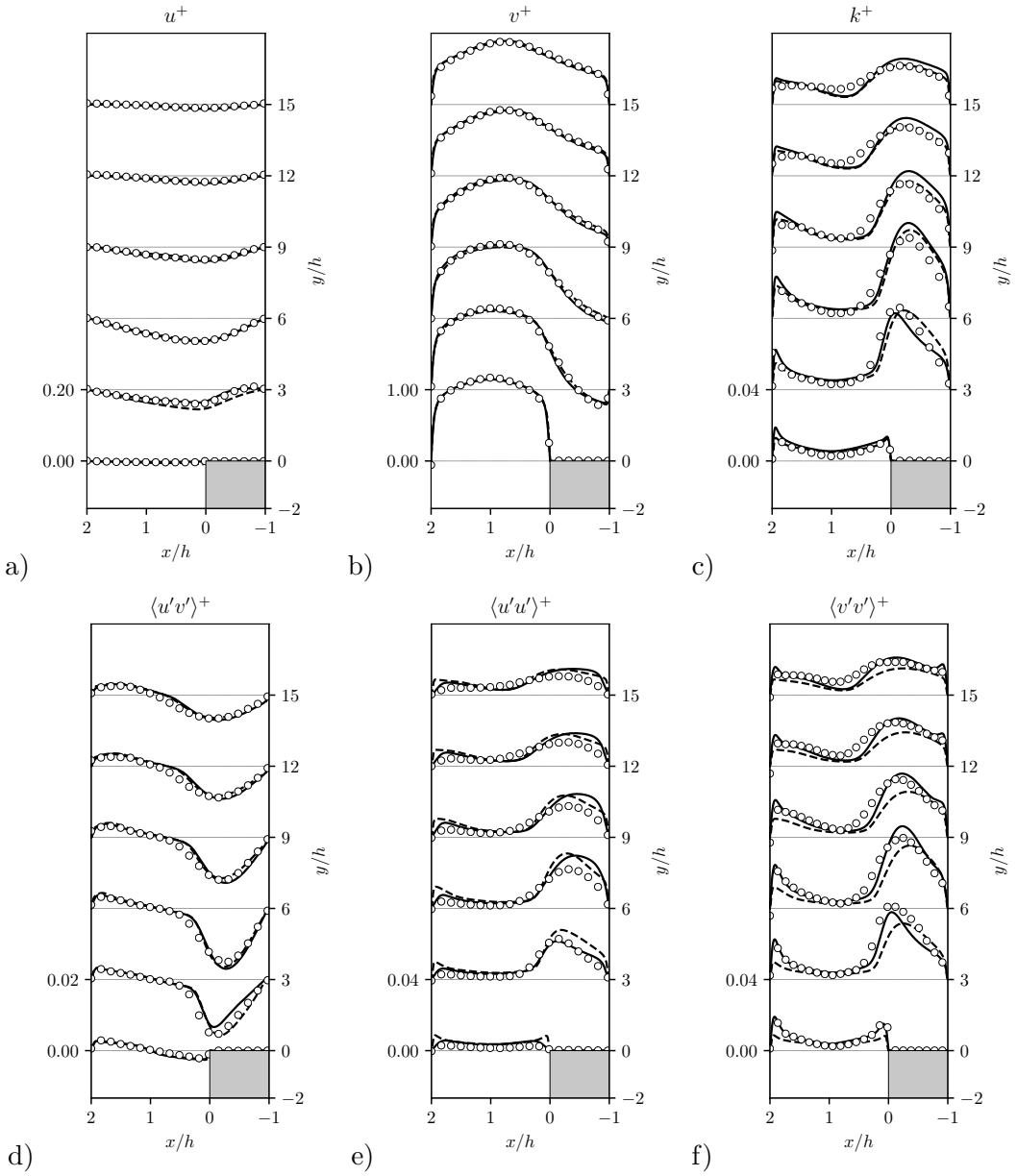

Figure 2: Simulation results with $Ri = 0$. Profile of dynamical fields: a) mean streamwise velocity v^+ b) mean wall-normal velocity u^+ c) turbulent kinetic energy k^+ d) shear stress $\langle u'v' \rangle^+$ e) normal stress $\langle u'u' \rangle^+$ f) normal stress $\langle v'v' \rangle^+$. —: Simulation results for anisotropic model; ----: Simulation results for isotropic model; ∘ : DNS data.

value is set at the inlet, i.e. $T_{in} = 423.15K$, and homogeneous Neumann conditions are used for the other boundaries except for the wall behind the step where a uniform heat flux $\dot{q}$ is imposed. For all the other turbulent variables, homogeneous Neumann conditions are set for both the inlet and outlet sections and the near wall behavior has been considered for the wall boundaries [10].

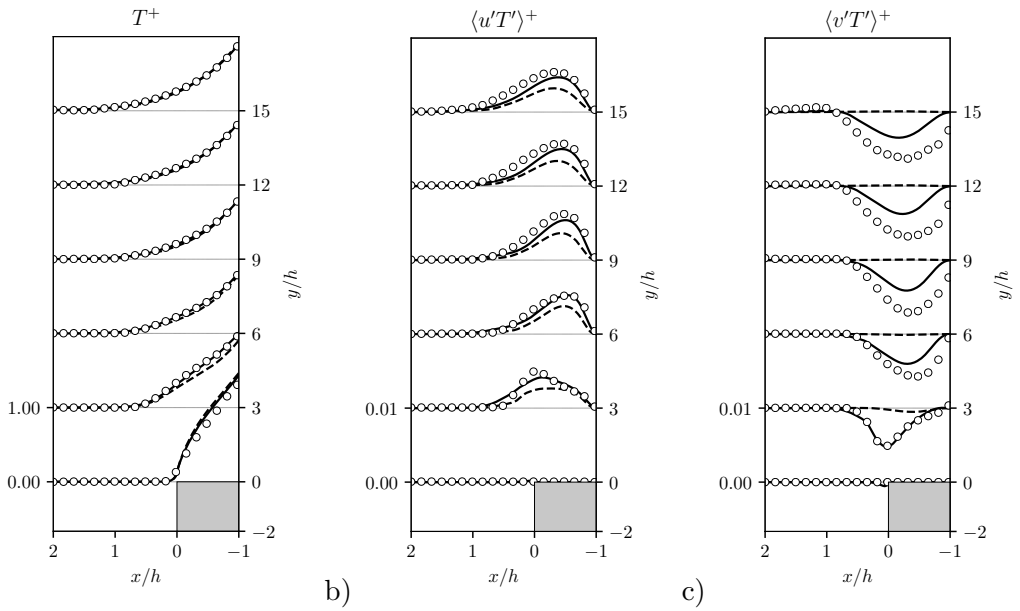

Figure 3: Simulation results with $Ri = 0.338$. Profile of thermal fields: a) mean temperature T^+ b) mean wall-normal turbulent heat flux $\langle u'T'\rangle^+$ c) mean streamwise turbulent heat flux $\langle v'T'\rangle^+$. —: Simulation results for anisotropic model; ----: Simulation results for isotropic model; ∘ : DNS data.

In this part, the results obtained with both the anisotropic (A4P) and isotropic (I4P) version of the proposed model, are compared with DNS data [13, 14, 15, 16], marked with circles in Figure 2, 3, 4, and 5. Here, the results for A4P model are reported using the solid line, while the dashed line represents the solution obtained with the I4P model. The isotropic model uses the Boussinesq Hypothesis for the evaluation of the Reynolds stress tensor, where the isotropic eddy viscosity is defined using the characteristic dynamical time scale, modelled as the expression (5). Moreover, in this model the evaluation of the turbulent heat flux is gained using the SDGH, where the isotropic eddy diffusivity is defined as $\alpha_t = C_\theta k \tau_m$ with τ_m given by (11).

Forced convection. For the forced convection case, the non-dimensional dynamical fields are reported in Figure 2 for several streamwise coordinate y/h values. The results for both the A4P and the I4P models are compared to the DNS data, available for the same non-dimensional coordinates [14]. The wall-normal $u^+ = u/U_b$ and the streamwise $v^+ = v/U_b$ velocity components, reported respectively in Figure 2a) and Figure 2b), present a good agreement when compared with the DNS results for both the anisotropic and the isotropic models. In addition, the non-dimensional turbulent kinetic energy $k^+ = k/U_b^2$, shown in Figure 1, is well reproduced by both models. In Figures 2d), 2e), and 2f), the non-dimensional components of the Reynolds stress tensor are reported in comparison with DNS data. These turbulent fields, obtained with the A4P model, present an overall good agreement with DNS data and show a slight improvement if compared to the isotropic model results, in particular regarding the diagonal components of the tensor. The non-dimensional thermal fields are shown in Figure 3, where $T^+ = (T - T_{ref})/\Delta T$ is the non-dimensional temperature, $\langle u'T'\rangle^+$, and $\langle v'T'\rangle^+$ are, respectively,

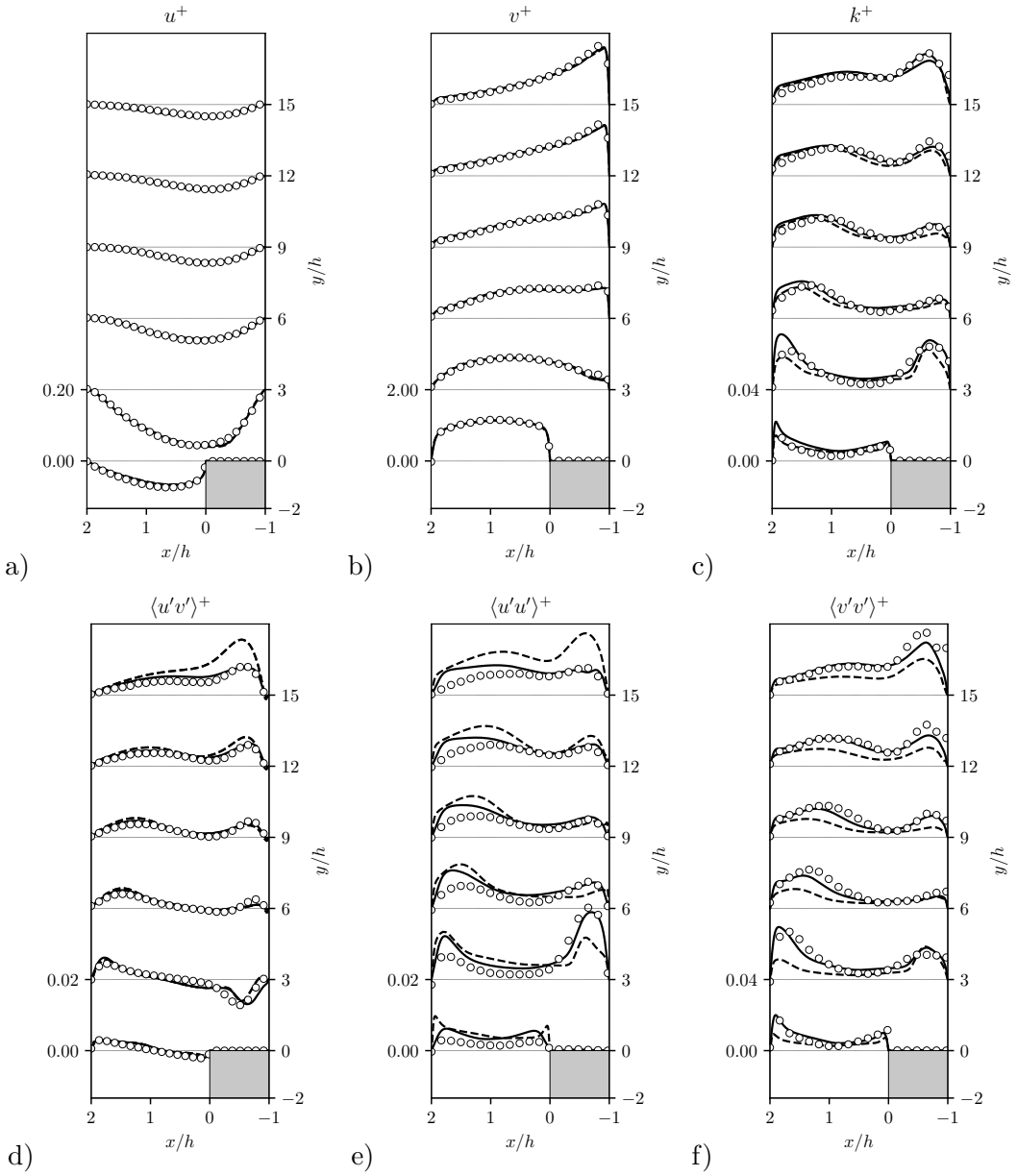

Figure 4: Simulation results with $Ri = 0.338$. Profile of dynamical fields: a) mean streamwise velocity v^+ b) mean wall-normal velocity u^+ c) turbulent kinetic energy k^+ d) shear stress $\langle u'v' \rangle^+$ e) normal stress $\langle u'u' \rangle^+$ f) normal stress $\langle v'v' \rangle^+$. —: Simulation results for anisotropic model; ----: Simulation results for isotropic model; ∘ : DNS data.

the non-dimensional wall-normal and the non-dimensional streamwise components of the turbulent heat flux. For the temperature profile (Figure 5a)), an overall good agreement with DNS data is obtained using both the anisotropic and isotropic models. The improvement given by the A4P model is well remarked in Figure 5b) and 5c), where the components of the turbulent heat flux are reported. Apart from a slight underestimation, the $\langle u'T' \rangle^+$ profile obtained with

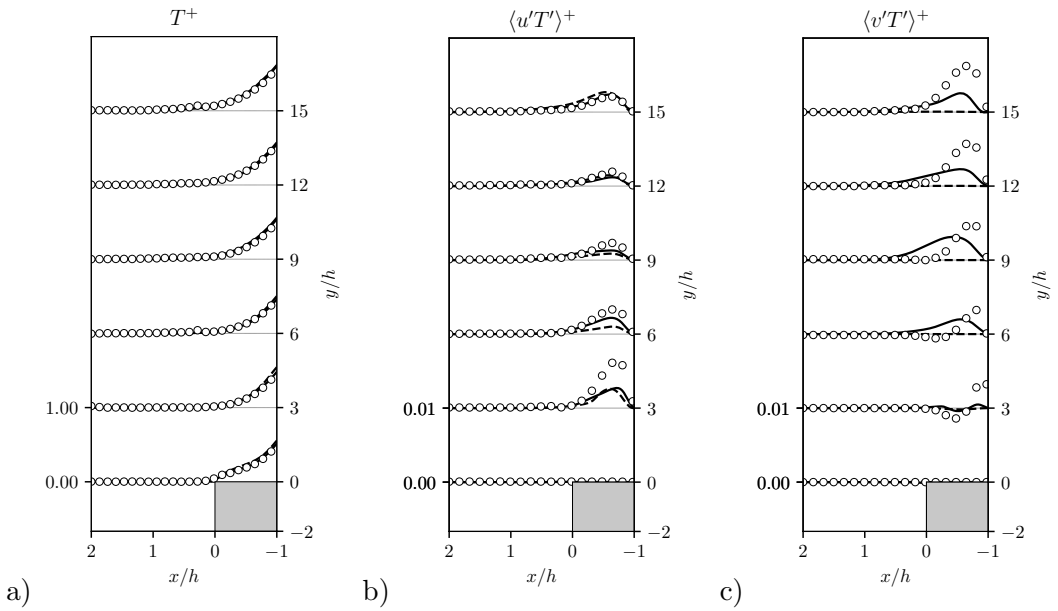

Figure 5: Simulation results with $Ri = 0$. Profile of thermal fields: a) mean temperature T^+ b) mean wall-normal turbulent heat flux $\langle u'T'\rangle^+$ c) mean streamwise turbulent heat flux $\langle v'T'\rangle^+$. —: Simulation results for anisotropic model; ----: Simulation results for isotropic model; ∘ : DNS data.

the A4P model is in good agreement with the benchmark if compared to the isotropic model results. Moreover, the A4P model provides better results for the streamwise component, which is, by contrast, totally underestimated by the I4P model.

Mixed convection. The same comparison, made for the forced convection case, is reported in this subsection in order to present the numerical results obtained with $Ri = 0.338$. As regards the mean velocity components $u^+ = u/U_b$ and $v^+ = v/U_b$, reported in Figure 4a) and Figure 4b), a good agreement with the DNS data can be obtained using both models. On the other hand, the A4P model helps to improve the prediction of all the three components of the Reynolds stress tensor when compared with the I4P model, as can be seen in Figures 4d), 4e), and 4f). The prediction of the temperature field, shown in Figure 5a), is in good agreement with the DNS data for both model simulations, although turbulent heat flux profiles do not strictly fit the benchmark results. Even if the streamwise component of the turbulent heat flux $\langle v'T'\rangle^+$ presents some discrepancies in correspondence of the near wall region, the anisotropic simulation provides better results than those of the I4P model. These differences with the DNS data are mainly due to the characteristic thermal time scale τ_m modelling, which should be improved in order to better predict the near wall behavior.

4 CONCLUSION

In this work, the simulation of turbulent liquid sodium flow over a vertical backward-facing step has been obtained using an anisotropic four-equation turbulence model. In order to evaluate the Reynolds stress tensor and turbulent heat flux, an Explicit Algebraic Stress Model (EASM)

and an Explicit Algebraic Heat Flux Model (EAHFM), respectively, have been adopted. In addition, the logarithmic four-equation turbulence model K-Ω-K_θ-Ω_θ, coupled with the algebraic models, has been used for the closure of the model. For both forced and mixed convection regimes, the results obtained with the proposed model have been compared to the isotropic version of the model and have been validated with literature DNS data. The prediction of the mean velocity and temperature profiles given by the new proposed model is in good agreement with the benchmark data. Moreover, for both the flow regimes, the anisotropic model presents a general enhancement in the representation of the Reynolds stress tensor, when compared to the previous isotropic model. As regards the turbulent heat flux components, the A4P model has brought significant improvements, in particular in the forced convection case. Despite some inaccuracies, the proposed model has provided promising results also in the mixed convection case, where there is plenty of scope for improvement.

REFERENCES

[1] A. Heinzel, W. Hering, J. Konys, L. Marocco, K. Litfin, G. Müller, J. Pacio, C. Schroer, R. Stieglitz, L. Stoppel, *et al.*, "Liquid metals as efficient high-temperature heat-transport fluids," *Energy Technology*, vol. 5, no. 7, pp. 1026–1036, 2017.

[2] L. Marocco, G. Cammi, J. Flesch, and T. Wetzel, "Numerical analysis of a solar tower receiver tube operated with liquid metals," *International Journal of Thermal Sciences*, vol. 105, pp. 22–35, 2016.

[3] D. Frazer, E. Stergar, C. Cionea, and P. Hosemann, "Liquid metal as a heat transport fluid for thermal solar power applications," *Energy Procedia*, vol. 49, pp. 627–636, 2014.

[4] S. Manservisi and F. Menghini, "Triangular rod bundle simulations of a cfd κ-ε-κ_θ-ε_θ heat transfer turbulence model for heavy liquid metals," *Nuclear Engineering and Design*, vol. 273, pp. 251–270, 2014.

[5] X. Cheng and N.-i. Tak, "Investigation on turbulent heat transfer to lead–bismuth eutectic flows in circular tubes for nuclear applications," *Nuclear Engineering and Design*, vol. 236, no. 4, pp. 385–393, 2006.

[6] A. Shams, A. De Santis, L. Koloszar, A. V. Ortiz, and C. Narayanan, "Status and perspectives of turbulent heat transfer modelling in low-prandtl number fluids," *Nuclear Engineering and Design*, vol. 353, p. 110220, 2019.

[7] A. De Santis and A. Shams, "Application of an algebraic turbulent heat flux model to a backward facing step flow at low prandtl number," *Annals of Nuclear Energy*, vol. 117, pp. 32–44, 2018.

[8] A. Shams and A. De Santis, "Towards the accurate prediction of the turbulent flow and heat transfer in low-prandtl fluids," *International Journal of Heat and Mass Transfer*, vol. 130, pp. 290–303, 2019.

[9] S. Manservisi and F. Menghini, "A cfd four parameter heat transfer turbulence model for engineering applications in heavy liquid metals," *International Journal of Heat and Mass Transfer*, vol. 69, pp. 312–326, 2014.

[10] R. Da Via, S. Manservisi, and F. Menghini, "A k-ω-k_θ-ω_θ four parameter logarithmic turbulence model for liquid metals," *International Journal of Heat and Mass Transfer*, vol. 101, pp. 1030–1041, 2016.

[11] R. Da Vià, V. Giovacchini, and S. Manservisi, "A logarithmic turbulent heat transfer model in applications with liquid metals for pr= 0.01–0.025," *Applied Sciences*, vol. 10, no. 12, p. 4337, 2020.

[12] R. Da Vià and S. Manservisi, "Numerical simulation of forced and mixed convection turbulent liquid sodium flow over a vertical backward facing step with a four parameter turbulence model," *International Journal of Heat and Mass Transfer*, vol. 135, pp. 591–603, 2019.

[13] M. Niemann and J. Fröhlich, "Direct numerical simulation of turbulent heat transfer behind a backward-facing step at low prandtl number," *PAMM*, vol. 14, no. 1, pp. 659–660, 2014.

[14] M. Niemann and J. Fröhlich, "Buoyancy-affected backward-facing step flow with heat transfer at low prandtl number," *International Journal of Heat and Mass Transfer*, vol. 101, pp. 1237–1250, 2016.

[15] M. Niemann and J. Fröhlich, "Turbulence budgets in buoyancy-affected vertical backward-facing step flow at low prandtl number," *Flow, Turbulence and Combustion*, vol. 99, no. 3, pp. 705–728, 2017.

[16] M. Niemann and J. Fröhlich, "Buoyancy effects on turbulent heat transfer behind a backward-facing step in liquid metal flow," in *Direct and Large-Eddy Simulation X*, pp. 513–519, Springer, 2018.

[17] K. Abe, T. Kondoh, and Y. Nagano, "On reynolds-stress expressions and near-wall scaling parameters for predicting wall and homogeneous turbulent shear flows," *International Journal of Heat and Fluid Flow*, vol. 18, no. 3, pp. 266–282, 1997.

[18] H. Hattori, A. Morita, and Y. Nagano, "Nonlinear eddy diffusivity models reflecting buoyancy effect for wall-shear flows and heat transfer," *International Journal of Heat and Fluid Flow*, vol. 27, no. 4, pp. 671–683, 2006.

[19] K.-i. Abe, T. Kondoh, and Y. Nagano, "A two-equation heat transfer model reflecting second-moment closures for wall and free turbulent flows," *International journal of heat and fluid flow*, vol. 17, no. 3, pp. 228–237, 1996.

[20] A. Chierici, G. Barbi, G. Bornia, D. Cerroni, L. Chirco, R. Da Vià, V. Giovacchini, S. Manservisi, R. Scardovelli, and A. Cervone, "Femus-platform: a numerical platform for multiscale and multiphysics code coupling," in *9th edition of the International Conference on Computational Methods for Coupled Problems in Science and Engineering (Coupled Problems 2021)*, 2021.